Ground-state phase diagram of a spin-orbit-coupled bosonic superfluid in an optical lattice

Zhu Chen[1,*] and Zhaoxin Liang[2,†]

[1]*National Key Laboratory of Science and Technology on Computational Physics, Institute of Applied Physics and Computational Mathematics, Beijing 100088, China*

[2]*Shenyang National Laboratory for Materials Science, Institute of Metal Research, Chinese Academy of Sciences, Wenhua Road, 72, Shenyang, China*

(Received 28 July 2015; revised manuscript received 30 October 2015; published 5 January 2016)

In recent experiments, spin-orbit-coupled (SOC) bosonic gases in an optical lattice have been successfully prepared into any Bloch band [Hamner *et al.*, Phys. Rev. Lett. **114**, 070401 (2015)], which promises a viable contender in the competitive field of simulating gauge-related phenomena. However, the ground-state phase diagram of such systems in the superfluid regime is still lacking. Here we present a detailed study of the phase diagram in an optically trapped Bose gas with equal-weight Rashba and Dresselhaus SO coupling. We identify four different quantum phases, which include three normal phases and a mixed phase, by considering the wave vector k_1, the longitudinal $\langle\sigma_z\rangle$, and the transverse $\langle\sigma_x\rangle$ spin polarizations as three order parameters. The ground state of normal phases is a Bloch wave with a single wave vector k_1, which can position in arbitrary regions in the Brillouin zone. By contrast, the ground state of the mixed phase is a superposition of two Bloch waves with opposite k_1, which, remarkably, may lack periodicity even though the system's Hamiltonian is periodic. This mixed phase in the lattice setting can be seen as the counterpart of the stripe phase associated with the uniform SOC gas. Furthermore, due to the lattice-renormalized SOC, the phase diagram of the model system becomes significantly different from the uniform case when the lattice strength grows. Finally, a scheme for experimentally probing the mixed phase using Bragg spectroscopy is proposed.

DOI: 10.1103/PhysRevA.93.013601

I. INTRODUCTION

Loaded into an optical lattice (OL), an ultracold quantum gas with spin-orbital coupling (SOC) [1–4] has been recently realized in the laboratory [5], which has stimulated significant interests and ongoing activity. The motivation behind these efforts is twofold. First, prompted by the analogy to the newly discovered topological insulator and the related topological orders in the condensed-matter physics [6–8], where the interplay of SOC and periodicity plays an important role, an optically trapped atomic gas with SOC promises controlled realization of exotic configurations with nontrivial topology [9–14]. Compared to the uniform case, adding an OL results in enhanced correlations, which in particular opens the possibility to explore the SOC physics in the strongly interacting limit. Second, recent work in atomic physics has shown that even the SOC *per se* can lead to exotic many-body ground states which bear no direct analogy in solid-state systems [1–4]. For example, the SOC can impact the quantum phase transition from a superfluid to a Mott insulator [9–14]. It also gives rise to an effective Dzyaloshinskii-Moriya interaction [14–16], which is crucial for realizing such novel magnetic phases as Skyrmion crystals.

Motivated by the ongoing experiments [5], the emphasis of recent efforts has shifted timely to an optically trapped atomic gas with equal Rashba and Dresselhaus SOC within the Gross-Pitaevskii framework. In the uniform space, a remarkable feature of a SOC Bose-Einstein condensate (BEC) in its ground state is the existence of a stripe phase [17–21], where the density profile exhibits periodic modulation with the period intrinsically determined by the system's parameters. Adding an external OL on top of such SOC system, as has been done in recent experiments [5], introduces an external periodic modulation. Thus an outstanding challenge along this line is to understand the competition between SOC and OL in determining the possible ground states.

In this paper, we study the ground-state phase diagram of an optically trapped BEC with equal-weight combination of Rashba and Dresselhaus type SOC. Our main findings are as follows. (1) We have identified four phases of the model system, including three normal phases with Bloch-type ground states, and one *mixed* phase whose ground state involves a superposition of two *Bloch states* with opposite wave vectors. This mixed phase can be seen as generalizing the striped phase of the uniform counterpart to the presence of optical lattice. (2) The size of the mixed phase in the phase diagram shrinks with increasing lattice strength. This is accompanied by a shift of the single-particle energy spectrum minimum to the edge of Brillouin zone (BZ), which results in strong modifications of the phase diagram. (3) We have derived the low-energy excitations of the mixed phase, based on which we propose an experimental probe of the mixed phase using Bragg spectroscopy.

This paper is organized as follows. In Sec. II, we describe our model system, and introduce the variational ansatz which allows us to find the ground state of the system. A detailed analysis of the resulting phase diagram is presented in Sec. III. Afterwards, a scheme for the experimental detection of the mixed phase is proposed in Sec. IV, followed by a brief discussion on experimental conditions in Sec. V. We conclude with a summary in Sec. VI.

II. OPTICALLY TRAPPED BEC WITH SOC

We consider a three-dimensional (3D) BEC with Raman-induced SOC in the following geometry: in the x direction, the

*cz-male@163.com
†zhxliang@gmail.com

BEC is trapped in an OL, while in the y and z directions, the confinement is sufficiently strong so that the atomic motion in these directions can be seen as frozen. At the mean-field level, the energy functional of our model system can be written as [17–23] (see Appendix A for the validity of mean-field treatment for the considered system)

$$H = \int d^3r \Big[\Psi^\dagger H_0 \Psi + \frac{g_{11}}{2}|\Psi_1|^4 + \frac{g_{22}}{2}|\Psi_2|^4 + g_{12}|\Psi_1|^2|\Psi_2|^2 \Big]. \quad (1)$$

Here, $\Psi = (\Psi_1, \Psi_2)^T$ denotes the two-component condensate wave function, $\int d^3r|\Psi|^2 = N$ describes the renormalization with N being the total number of atoms, and $g_{ij} = 4\pi\hbar^2 a_{ij}/m$ $(i,j = 1,2)$ labels the interaction strength with a_{ij} being the s-wave scattering length between atoms in individual internal states. In addition, H_0 is a single-particle Hamiltonian which reads as

$$H_0 = \frac{1}{2m}[(p_x - \hbar k_R \sigma_z)^2 + p_\perp^2] + \frac{\Omega}{2}\sigma_x + \frac{\delta}{2}\sigma_z + \frac{m\omega_\perp^2}{2} \times \Big[\Big(y - \frac{d}{2}\sigma_z\Big)^2 + \Big(z - \frac{d}{2}\sigma_z\Big)^2 \Big] + V_0 \sin^2(k_L x). \quad (2)$$

Here $\sigma_{x(z)}$ labels the standard Pauli matrices and m is the bare atom mass. In addition, $\omega_\perp$ is the transverse trapping frequency of a spin-dependent harmonic potential, which confines the spin-up and spin-down condensate wave function near two positions displaced by a distance d along the y and z directions.

The above microscopic model is motivated by recent experiments [5] where Hamiltonian of the form (2) can arise as follows. First, the SOC with equal Rashba and Dresselhaus contributions [24–27] has been realized by coupling two hyperfine states of ^{87}Rb via a Raman process characterized by a momentum transfer $2\hbar k_R$, a coupling strength Ω, a two-photon detuning δ, and the corresponding recoil energy $E_R = \hbar^2 k_R^2/2m$; then, the SOC BEC is loaded adiabatically into a conventional optical lattice formed by two counterpropagating laser beams, which align with the Raman beams [5]. Here, k_L is the wave vector of the lattice beams with $E_L = \hbar^2 k_L^2/2m$ being the recoil energy and V_0 the lattice strength. In addition, the harmonic trapping potential along the x direction is very weak compared to the strength of lattice, and therefore will be ignored in our subsequent analysis.

Due to the strong transverse confinement, the BEC is frozen to the ground state of the harmonic trap along these directions. This allows a decomposition of the condensate wave function of the form $\Psi(\mathbf{r}) = \psi^T(x)\phi(y,z)$ with $\phi = (\phi_-, \phi_+)^T$, where $\phi_\pm = 1/(\sqrt{\pi}a_\perp)e^{-[(y\pm d/2)^2+(z\pm d/2)^2]/2a_\perp^2}$ with $a_\perp = \sqrt{\hbar/(m\omega_\perp)}$ [28], which, as we now show, permits our model system to be effectively described by an effective 1D energy functional. We first rescale the energy functional (1) into a dimensionless form with $x \to 2k_L x$, $\Omega \to \Omega e^{-d^2/2a_\perp^2}/8E_L$, $\delta \to \delta/8E_L$, $v = -V_0/16E_L$, $c_{ij} = \frac{N\hbar\omega_\perp k_L a_{ij}}{4\pi N_d E_L}(i = j)$, $c_{ij} = \frac{N\hbar\omega_\perp k_L a_{ij}}{4\pi N_d E_L} e^{-d^2/a_\perp^2}(i \neq j)$, $\gamma = k_R/2k_L$, and $\psi(x) \to \sqrt{n}\psi(x)$ [$n = N/L_x$ with L_x the condensate size in the x directions and N the total number of atoms; N_d is the number of lattice wells]. Assuming a spin asymmetric interaction with $c_{11} = c_{22} = c$ and $\delta = 0$, we substitute the above ansatz into (1) and, after integrating out $\phi(y,z)$, we obtain an effective 1D mean-field energy functional of the form

$$H = \frac{1}{L_x}\int_{-L_x/2}^{L_x/2} \Big\{ \psi^\dagger \Big[\frac{(p_x - \gamma\sigma_z)^2}{2} + \frac{\Omega}{2}\sigma_x + v\cos(x) \Big]\psi + \frac{c}{2}(|\psi_1|^4 + |\psi_2|^4) + c_{12}|\psi_1|^2|\psi_2|^2 \Big\} dx, \quad (3)$$

with the normalization $(1/L_x)\int_{-L_x/2}^{L_x/2}(|\psi_1|^2 + |\psi_2|^2)dx = 1$. Based on Eq. (3), the ground-state phase diagram of an optically trapped BEC with SOC is governed by the interplay among five parameters: the SOC parameters of γ and Ω, the interaction parameters of c and c_{12}, and the lattice strength v.

Before investigating the effects of an OL on the ground-state phase diagram, we first briefly review some important features of a SOC BEC in the uniform space, corresponding to Eq. (3) with $v = 0$. There, an exact ground state of the energy functional (1) exists for a noninteracting system ($c = c_{12} = 0$) which takes the form $\psi = \sqrt{n}(-\sin\theta, \cos\theta)^T e^{ik_1 x}$, with $\cos\theta = R/\sqrt{1+R^2}$, $R = \Omega/2(k_1 + \sqrt{k_1^2 + \Omega^2/4})$, and $k_1 = \pm\sqrt{\gamma^2 - \Omega^2/4\gamma^2}$ ($\Omega < 2\gamma$) or $k_1 = 0$ ($\Omega > 2\gamma$). Depending on the strength of the Raman coupling Ω, this ground state can be either in the "zero momentum" phase with $k_1 = 0$ and $\langle\sigma_z\rangle = 0$, where the BEC tends to condense into the zero momentum state, or in the "plane-wave phase" with $k_1 \neq 0$ and $\langle\sigma_z\rangle \neq 0$ which exhibits broken Z_2 symmetry. Turning on an asymmetric interaction ($c_1 = c_2 > c_{12}$) gives rise to a competition between the kinetic energy and spin-density interaction. As a result, a stripe phase can arise, which is favored for small Ω. The corresponding ground-state wave function is a superposition of two plane waves with opposite wave vectors [see Eq. (5) below]. Note that both the double-minimum structure in the single-particle energy spectrum and the spin-dependent interatomic interaction are crucial for the emergence of stripe phase.

Adding an additional OL ($v \neq 0$) to the above SOC BEC in the uniform space introduces an external spatial periodic modulation, which leads to two immediate consequences: first, the plane waves [see Eq. (5) below] are Bragg refracted to form Bloch waves [see Eq. (4) below]; second, the energy spectrum forms a Bloch band where an energy gap opens at the edge of the Brillouin zone. Thus intuitively we expect that (1) the action of an OL on the stripe phase of a SOC BEC in the uniform space will cause Bragg refraction of the two plane-wave components into the Bloch waves, giving rise to a ground state that is a *superposition of Bloch waves* with opposite wave vectors. (2) The modification of OL to the ground state of the uniform case will strongly depend on how close the energy minima $k_{\min}$ is to the edge of the Brillouin zone. In the limit of small Raman coupling, the momentum associated with the energy minima is $k_{\min} \sim \gamma$. For $\gamma \ll 1/2$, $k_{\min}$ is a distance away from the band edge. In this case, the minima configuration in the energy spectrum is qualitatively similar as its uniform counterpart, i.e., the energy spectrum is robust against the effect of OL. This can also be qualitatively understood from the renormalized mass picture: the effect of a weak OL gives rise to an effective mass m^* and an effective interaction $\tilde{c}$, such that the optically trapped system can be seen as a uniform fluid with lattice-renormalized parameters. By

contrast, when γ grows to become $\gamma \sim 1/2$, $k_{\min}$ shifts toward the band edge. There, the minima configuration becomes strongly altered by the OL, and we expect significant effect of an OL on the ground state.

The above intuitive understanding into the effect of an OL on a SOC BEC motivates us to write down an ansatz for the ground state of (3) which reads as

$$\psi_t = \psi_{k_1} + \psi_{-k_1} = \sum_m \left\{ \begin{pmatrix} a_{1m} \\ b_{1m} \end{pmatrix} e^{i(k_1+m)x} + \begin{pmatrix} a_{2m} \\ b_{2m} \end{pmatrix} e^{i(-k_1+m)x} \right\}. \quad (4)$$

Here, $\psi_{\pm k_1}$ are Bloch functions with wave vector $\pm k_1$ and $\{a_{im}, b_{im}, i = 1,2\}$ are the corresponding Fourier expansion coefficients. Using Eq. (4) to minimize the energy functional (3) under the normalization condition $\sum_{i,m} |a_{im}|^2 + |b_{im}|^2 = 1$, we can find the variational parameters and thus determine the ground state. The ansatz (4) allows us to capture the competition between the stripe phase and the external periodic modulation due to OL as follows. (i) When $\gamma \neq 0$ and $v = 0$, corresponding to a SOC Bose gas in free space, the expansion series is limited to $m = 0$. In this case, the coefficients $\{a_{i0}, b_{i0}\}(i = 1,2)$ can be chosen as $a_{10} = C_1 \cos\theta, b_{10} = -C_1 \sin\theta, a_{20} = C_2 \sin\theta$, and $b_{20} = -C_2 \cos\theta$ with $|C_1|^2 + |C_2|^2 = 1$. The ansatz (4) then reduces to

$$\psi_t = \sqrt{n}\left[C_1 \begin{pmatrix} \cos\theta \\ -\sin\theta \end{pmatrix} e^{ik_1 x} + C_2 \begin{pmatrix} \sin\theta \\ -\cos\theta \end{pmatrix} e^{-ik_1 x} \right], \quad (5)$$

which recovers exactly Eq. (3) in Ref. [18]. (ii) When $v \neq 0$ and $\gamma = 0$, corresponding to an optically trapped Bose gas without SOC, the ansatz (4) trivially describes a Bloch state with a period of 2π. (iii) For $\gamma \neq 0$ and $v \neq 0$, when the SOC interplays with OL, we see that the atoms can condense into a state that is a superposition of two Bloch waves with opposite wave vectors of $\pm k_1$. The density profile of this state exhibits a SOC-induced periodic modification with the period depending on k_1, aside from the period 2π due to the lattice. We remark that in writing down the ansatz (4), we have ignored higher-order harmonics with wave vectors like $\pm 3k_1$, $\pm 5k_1$, etc. [18,20,21], which can be justified for our case (see detailed discussions in Appendix B).

In determining the ground-state phase diagram of the energy functional (3), we stress the existence of three order parameters: the wave vector k_1, the longitudinal spin polarization $\langle \sigma_z \rangle$, and the transverse polarization $\langle \sigma_x \rangle$ defined by

$$\langle \sigma_{z/x} \rangle = \frac{1}{L_x} \int_{L_x/2}^{L_x/2} \psi^\dagger \sigma_{z/x} \psi \, dx. \quad (6)$$

Depending on the interplay among the three order parameters, we identify four phases in the ground-state phase diagram as follows.

Phase I, the mixed phase, where both components $\psi_{\pm k_1}$ exist with $k_1 \neq 0$, $\sigma_z = 0$, and $\sigma_x \neq 0$. The ground state is a superposition of two Bloch waves with opposite wave vectors.

Phase II, the separated phase with $0 < |k_1| < 1/2$, $\sigma_z \neq 0$, and $\sigma_x \neq 0$. The ground state is described by a Bloch wave with both nonzero longitudinal and transverse spin polarizations.

Phase III, a single momentum phase with $k_1 = 0$, $\sigma_z = 0$, and $|\sigma_x| = 1$, where the spin along x direction is fully polarized.

Phase IV, a single momentum phase with $k_1 = 1/2$, $\sigma_z = 0$, and $\sigma_x \neq 0$, which has no counterpart in the uniform case and arises uniquely from the periodic modulation.

III. GROUND-STATE PHASE DIAGRAM

In the previous section, we have developed the intuitive physical picture and predicted features in the ground state of an optically trapped SOC BEC compared to the uniform case. Below we derive the complete ground-state phase diagram (see Fig. 1) by numerically minimizing the energy functional (3)

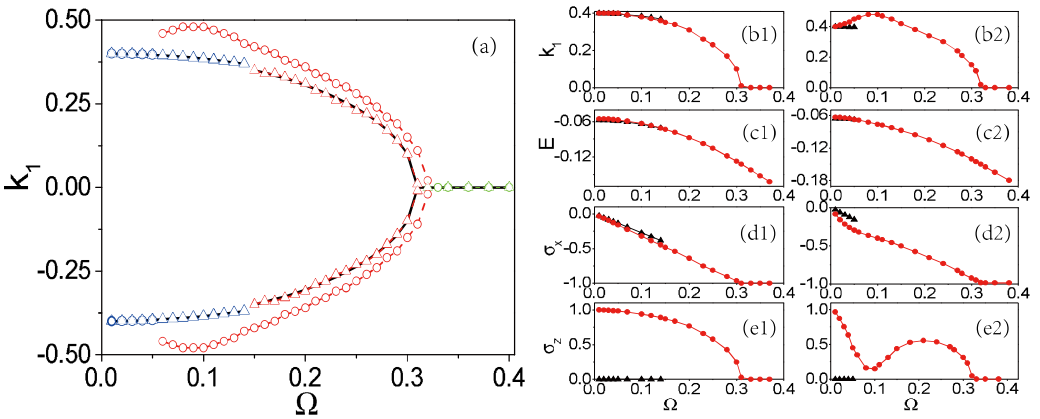

FIG. 1. Ground-state phase diagram of SOC bosonic superfluid in an OL. The k_1 and Ω (or E) are in units of $2k_L$ and $8E_L$, respectively. Left panel: (a) lattice-modified ground-state phase diagram in the Ω-k_1 plane with $v = -V_0/16E_L = 0$ (black solid curves), $v = -V_0/16E_L = 0.01$ (open triangles), and $v = -V_0/16E_L = 0.1$ (open circles). Different colored curves correspond to the different quantum phases, i.e., green curves: zero momentum phase or normal phase; red curves: separated phase or plane-wave phase; blue curves: mixed phase or stripe phase. Right panel: subplots are physical quantities of k_1 [(b1) and (b2)], energy density E [(c1) and (c2)], transverse and longitudinal spin polarization $\langle \sigma_x \rangle$ [(d1) and (d2)] and $\langle \sigma_z \rangle$ [(e1) and (e2)] for single momentum as well as the mixed phase states with respect to Ω with the parameters of $v = -V_0/16E_L = 0.01$ for (b1)–(e1) and $v = -V_0/16E_L = 0.1$ for (b2)–(e2), respectively. Here, red circles correspond to the plane-wave phase and black triangles represent the mixed phase. Other dimensionless parameters are $\gamma = k_R/2k_L = 0.4$, $c = N\hbar\omega_\perp k_L a_{11}/(4\pi N_d E_L) = 0.05$, and $c_{12} = N\hbar\omega_\perp k_L a_{12}/(4\pi N_d E_L) e^{-d^2/a_\perp^2} = 0.04$.

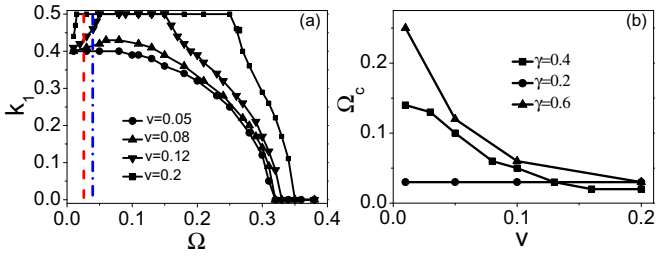

FIG. 2. Effects of lattice strength v on the ground-state phase diagram. The k_1, Ω, and v are in units of $2k_L$, $8E_L$, and $-16E_L$, respectively. (a) The wave vector of k_1 as a function of Ω for various lattice strength with $v = 0.05$ (circles), $v = 0.08$ (upper triangles), $v = 0.12$ (lower triangles), and $v = 0.20$ (squares). Red dashed line: the critical value of Ω at which the transition into the phase (IV) occurs for $v = 0.2$; blue dash-dot line: critical value of Ω when $v = 0.12$. (b) The critical value of Ω when the phase transition from phase (I) to phase (II) occurs, for $\gamma = k_R/2k_L$ with $\gamma = 0.6$ (triangles), $\gamma = 0.4$ (squares), and $\gamma = 0.2$ (circles), respectively. Other parameters are $c = N\hbar\omega_\perp k_L a_{11}/(4\pi N_d E_L) = 0.05$ and $c_{12} = N\hbar\omega_\perp k_L a_{12}/(4\pi N_d E_L)e^{-d^2/a_\perp^2} = 0.04$.

using anstaz (4). In particular, we will show how an OL can affect the momentum minima k_1 (see Fig. 2) which plays a key role in determining the phase diagram, and the density dependence in the phase diagram (see Fig. 3). We will refer to a weak OL as the case when $V_0 \ll E_L$ with E_L being the recoil energy (e.g., $v = -V_0/16E_L = 0.01$), and a strong lattice as the case when $V_0 \sim E_L$ (e.g., $v = -V_0/16E_L = 0.1$). We also note that for a BEC trapped in an OL, there exist two different

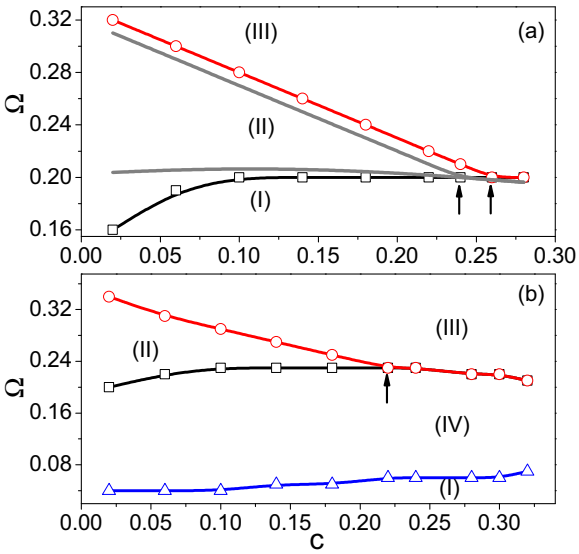

FIG. 3. Ground-state phase diagram in the Ω-c plane with $(c - c_{12})/c = 1/3$ being fixed. The Ω is in units of $8E_L$ and $c = 1/(4\pi)(k_L a_{11})\frac{\hbar\omega_\perp}{E_L}\frac{N}{N_d}$. Different phases are labeled and separated by the solid lines, which are fitting curves of the numerical data (i.e., the squares, circles, and triangles). (a) There exist three phases, two phase transitions, and a tricritical point for $\gamma = k_R/2k_L = 0.4$ and $v = -V_0/16E_L = 0.05$. (b) There are four phases and three phase transitions for $\gamma = k_R/2k_L = 0.4$ and $v = -V_0/16E_L = 0.12$. The tricritical points are marked by arrows.

types of instabilities that can break the superfluidity of the system, dynamical instability and Landau instability [29–31], both of which have been extensively studied in theories [29–31] and experiments [32,33]. To avoid the instability problem, in our calculations we have limited ourselves within the stable parameter regime.

We begin with discussing the effect of an OL on the ground-state phase diagram of a SOC BEC with fixed interaction strength. As a benchmark for later analysis, we recall the phase diagram of the uniform case ($v = 0$) where analytical expressions exist [18]: $k_1 = \gamma\sqrt{1 - \Omega^2/[4F(\beta,c,c_{12})]}$ with $F(\beta,c,c_{12}) = \gamma^2 - (1 - 4\beta)(c - c_{12})n/2 + \beta(c + c_{12})n$ (depending on whether the system is in the stripe phase or not, β takes the value of $1/4$ or 0). Our numerical results for $v = 0$ are clearly consistent with those in Refs. [24,25] [solid black curves in Fig. 1(a)]. In the presence of a weak OL, our results [$v = 0.01$, see the curve with open triangles in Fig. 1(a)] are seen to barely deviate from the uniform counterpart ($v = 0$). This is because here the particle energy minima locate at $\pm\gamma = \pm 0.4$. As discussed earlier, for such case a weak perturbation from OL will barely influence the position of the minima, instead, it only renormalizes the mass m^* and interaction coupling $\tilde{c}$ and $\tilde{c}_{12}$. By contrast, notable changes in the phase diagram are observed with increasing lattice strength [see $v = 0.1$, the curves with open circles in Fig. 1(a)], including the relative sizes of the mixed phase [blue curves in Fig. 1(a)], the zero momentum phase [green curves in Fig. 1(a)], and the behavior of k_1 for the separated phase [red curves in Fig. 1(a)].

To gain more insight into each phase and the corresponding phase transitions, we have plotted the wave vector k_1, the energy density E, and the spin polarizations $\langle\sigma_x\rangle$ and $\langle\sigma_z\rangle$ as a function of Ω for a weak OL ($v = 0.01$) [Figs. 1(b1)–1(e1)], and a strong OL ($v = 0.1$) [Figs. 1(b2)–1(e2)], respectively. We see that the system favors the mixed phase in the limit of weak Raman coupling Ω. When Ω grows, a competition arises between the mixed phase (I) and the separated phase (II), with a phase transition from (I) to (II) revealed by the energy subplot. Further increase of Ω leads to a transition from the separated phase (II) to the zero-momentum phase (III), which can be clearly seen in the k_1 and σ_z subplots. In addition, by comparing Figs. 1(b1) with 1(b2), we conclude that the critical value for the onset of the transition from the separated phase to the zero-momentum phase is insensitive to the increase of v.

For both cases of weak and strong optical lattices, the global phase diagrams show several features that are similar to their uniform counterpart: the transitions from the phase (I) to (II) and from (II) to (III) occur successively, which are accompanied by a jump of $\langle\sigma_z\rangle$ and $\langle\sigma_x\rangle$ for the first transition. Yet remarkably, different features arise in the case with strong OL: the size of the mixed phase is seen to shrink significantly [Figs. 1(b1) and 1(b2)], while the value of k_1 in the separated phase shows an anomalous increase and shifts toward the band edge when Ω grows, accompanied by a dip in σ_z toward $\sigma_z = 0$. This is due to the increasingly pronounced role of OL on modifying the single particle spectrum in the region near the band edge. For example, when $\gamma = 0.4$, the single particle minimum is not well separated from the band edge, and therefore is more susceptible to a relative strong OL. We

stress that this phenomenon can be seen as a signature for the emergence of phase IV. Further increase in the lattice strength will cause k_1 to reach the band edge ($k = 1/2$), with $\langle\sigma_z\rangle = 0$. We expect the existence of phase IV and transition from phase (II) to phase (IV). Interestingly, when $\gamma \sim 1/2$, the ground state is a Bloch wave with $k \sim 1/2$ which does not suffer from the instability problem typically occurring to a Bloch wave at the band edge.

To further verify above conjecture about the new phase IV, we have plotted the momentum minimum k_1 as a function of Ω for various lattice strength v, as illustrated in Fig. 2(a). We clearly see that for a sufficiently strong lattice, a plateau is formed at $k_1 = 1/2$, which enlarges when v further increases. This results in significant modification in the phase structure of the system: On one hand, since one more phase emerges compared to the weak lattice case, there can exist four phase transitions with increasing Ω, i.e., (I)−(II)−(IV)−(II)−(III), as illustrated by the case of $v = 0.12$ (blue dash-dot line in the left panel of Fig. 2). On the other hand, the growth of the phase (IV) may cause one or both of the phase (II)s to vanish, thus reduce the number of phase transitions from four to three, even to two. This is observed in the $v = 0.2$ case (red dashed line in the left panel of Fig. 2), where three phase transitions exist, i.e., (I)−(IV)−(II)−(III).

In addition, from the anstaz (4) and Fig. 1 we have seen that the effect of OL on the phase diagram becomes more pronounced when k_1 (or γ) approaches $1/2$. To gain more insight into this, we have plotted the critical value of Ω_c taken from phase (I) to phase (II) as a function of the lattice strength v (see the right panel of Fig. 2) for two cases: when γ is away from $1/2$, e.g., $\gamma = 0.2$, and when $\gamma \sim 1/2$, e.g., $\gamma = 0.4$ and $\gamma = 0.6$. For both $\gamma = 0.4$ and $\gamma = 0.6$, we see that Ω_c is sensitive to the strength of OL, showing a monotonous decrease for increasing v and asymptotically saturates to the same value for large v. By contrast, for $\gamma = 0.2$, Ω_c is almost constant with respect to the increasing lattice strength, indicating a robust phase diagram against the lattice induced periodic modulation. In this case, the ground-state properties resemble its uniform counterpart and the phase (IV) never appears.

Equipped with the above understanding into the effect of OL on the phase diagram of the model system, we conclude this section with the discussion on the effect of interaction, as illustrated in Fig. 3. As stated earlier, the phase diagram for a weak v is qualitatively similar as its uniform space counterpart. This is also clearly seen in Fig. 3(a). There, the transition lines show a similar structure as that in uniform space (i.e., the gray lines) with slight deviation, which only becomes visible for large c. As a result, the tricritical points are close to each other. However, for deeper lattice as shown in Fig. 3(b), the phase diagram experiences a drastic change due to the emergence of one more phase, i.e., phase (IV). The phase (IV) separates phase (I) from (II) and (III), leading to at most three phase transitions in this system. A tricritical point is shown to exist, however, among phases (II, III, and IV), which has no counterpart in the uniform space. One may conjecture that another tricritical point among phase (I, III, and IV) might arise from the trend of the triangles and circles by further increasing c, the discussion of which is however beyond the scope of the present paper.

IV. EXPERIMENTAL DETECTION

In this section we briefly discuss the experimental identification of different phases predicted in this work. We will focus on the case of mixed phase as other phases can be distinguished by measuring the wave vector k_1 [24,25]. Note that even in the uniform space, a direct experimental detection of the stripe phase is currently an outstanding challenge due to the relative small stripe separation in the density profile and the finite resolution capability [24,25]. In this direction, a recent paper from Stringari's group [21] has proposed to increase the fringe contrast by reducing the effective interspecies interaction while increasing the wavelength of the fringe with a Bragg pulse, which may put their experimental detection in a realistic perspective.

Here, we consider an alternative route to probe the mixed phase, using Bragg spectroscopy as a way to measure the corresponding excitation energy [34–38]. At the heart of our proposal with Bragg spectroscopy is the measurement of the dynamic structure factor of a SOC BEC, i.e., the response of a BEC to the external density perturbation generated by the Bragg beam (in this sense the role of Bragg beam in our scheme is different from Ref. [21] where a $\pi/2$ Bragg pulse is used to cause the increase of the fringe wavelength). Denoting the linear perturbation by $V_1 = \frac{V}{2}[\rho_{\mathbf{q}}^\dagger e^{-i\omega t} + \rho_{-\mathbf{q}} e^{+i\omega t}]$, where $\rho_{\mathbf{q}} = \sum_j e^{i\mathbf{q}\cdot\mathbf{r}_j/\hbar}$ is the Fourier transformed one-body density operator with $\mathbf{q} = \mathbf{k}_1 - \mathbf{k}_2$ the probe momenta, the dynamical structure factor takes the form [35]

$$S(\mathbf{q},\omega) = \sum_e |\langle e|\rho_{\mathbf{q}}^\dagger|0\rangle|^2 \delta(\omega - (E_e - E_g)/\hbar). \tag{7}$$

Here $|0\rangle$ ($|e\rangle$) is the ground (excited) state having the energy E_g (E_e) and $Z_e = |\langle e|\rho_{\mathbf{q}}^\dagger|0\rangle|^2$ the excitation strength. The knowledge of dynamic structure factor then allows a direct probe of the excitation spectrum of the system.

Our goal is thus to calculate the excitation spectrum and the dynamic structure factor $S(q,\omega)$ of the model system in the mixed phase within the Bogoliubov framework [22,39,40]. Specifically, the condensate wave function $(\psi_1,\psi_2)^T$ can be decomposed into the ground-state wave function $(\phi_{\uparrow 0},\phi_{\downarrow 0})^T$ and a small fluctuating term, reading

$$\begin{pmatrix}\psi_1\\ \psi_2\end{pmatrix} = e^{-i\mu t}\left[\begin{pmatrix}\phi_{\uparrow 0}\\ \phi_{\downarrow 0}\end{pmatrix} + \begin{pmatrix}u_\uparrow(x)\\ u_\downarrow(x)\end{pmatrix}e^{-i\omega t} + \begin{pmatrix}v_\uparrow^*(x)\\ v_\downarrow^*(x)\end{pmatrix}e^{i\omega t}\right]. \tag{8}$$

Substituting Eq. (8) into the Gross-Piteavskii equation and keeping the first-order terms, we obtain the Bogoliubov–de Gennes (BdG) equation [22,39–41],

$$\begin{pmatrix}A & B\\ -B^* & -A^*\end{pmatrix}\begin{pmatrix}u\\ v\end{pmatrix} = \omega\begin{pmatrix}u\\ v\end{pmatrix}. \tag{9}$$

Here $u = (u_\uparrow,u_\downarrow)^T$, $v = (v_\uparrow,v_\downarrow)^T$, and matrices A and B are given by

$$A = \begin{pmatrix}T_- + 2c|\phi_{\uparrow 0}|^2 + c|\phi_{\downarrow 0}|^2 & c_{12}\phi_{\uparrow 0}\phi_{\downarrow 0}^* + \frac{\Omega}{2}\\ c_{12}\phi_{\uparrow 0}^*\phi_{\downarrow 0} + \frac{\Omega}{2} & T_+ + 2c|\phi_{\downarrow 0}|^2 + c|\phi_{\uparrow 0}|^2\end{pmatrix},$$
$$B = \begin{pmatrix}c\phi_{\uparrow 0}^2 & c_{12}\phi_{\uparrow 0}\phi_{\downarrow 0}\\ c_{12}\phi_{\uparrow 0}\phi_{\downarrow 0} & c\phi_{\downarrow 0}^2\end{pmatrix}, \tag{10}$$

with $T_{\mp} = -\partial_x^2/2 \pm i\gamma\partial_x + v\cos(x) - \mu$. Note that in the normal phase, $u(x)$ and $v(x)$ can be taken as Bloch-type so that a solution of the BdG equation is viable through a Fourier decomposition as in Eq. (4). However, in the mixed phase, the effective potential takes the form $v\cos(x) + |\psi|^2$, which involves two periodic functions: an external period 2π due to lattice and an intrinsic period π/k_1 due to SOC. (i) If the two periods are commensurate, we can always express k_1 by a rational number $s/2t$, with $s < t$ being coprime integers. As such, the ground state is still a Bloch wave. The band structure of the excitation spectrum is preserved, but each excitation band of a lattice-free SOC gas will split into t subbands. (ii) On the other hand, it is possible that the two aforementioned periods become incommensurate. When this occurs, the ground state will be no longer Bloch wave and the excitation spectrum turns out to be pointlike. For both cases, the band-splitting manifests itself in the *discretization* of the dynamical structure factors Z_n, especially the low energy part. We emphasize that in the present work, k_1 is determined numerically, which actually leads to the prohibition of the determination of optimal s and t as well as the determination of the commensuration of the two periods. To circumvent this difficulty, and to be more in line with experiments where the condensate always resides in external trap with finite dimension, we consider a system trapped in a weak harmonic trap $\frac{1}{2}m\omega_x^2x^2$ with ω_x being trap frequency. This way Eq. (9) can be solved by a discretization in the real space, i.e., $\psi_0 = \sum_n \psi_n\delta(x - n\delta x)$, which can be obtained by the imaginary-time evolution method. Correspondingly, $u(x) = \sum_n u_n\delta(x - n\delta x)$, $v(x) = \sum_n v_n\delta(x - n\delta x)$, and

$$Z(q,j) = \left| \int dx\, e^{iqx/\hbar}(u_j^\dagger\phi_0 + \phi_0^\dagger v_j^*) \right|^2. \qquad (11)$$

Note that while the momentum $\hbar q$ is no longer a good quantum number [35], the momentum transferred by Bragg refraction is well defined. When the wavelength of the perturbation is smaller than the linear size of the condensate, the linear response is supposed to resemble its uniform space counterpart, which implies $q > \sqrt{\omega_x}$ [42–44].

Before proceeding, it is instructive to briefly recall some recent work on the dynamic and static structure factors of the stripe phase of a SOC BEC in the uniform case [20], as well as in the plane-wave phase and zero-momentum phase of a SOC BEC in an OL [22]. As pointed by Ref. [20], a band structure featuring a vanishing excitation energy and a divergent behavior of the structure factor at the Brillouin wave vector can be seen as an unambiguous evidence for the characteristic density modulations of the stripe phase. In Ref. [22], the linear-to-quadratic crossover in both the low-energy spectrum and the static structure factor presents a striking manifestation of the transition from an ordinary band to a flat band of a SOC BEC in an OL. Experimentally, Bragg spectroscopy has been recently used to reveal the structure of the excitation spectrum in a BEC with SOC in free space [45–47]. In particular, the measurement of the static structure factor combined with Feynman's relation has allowed the experimental verification of the roton-maxon dispersion in these systems. As we will see, this work complements our present study, and altogether provides a complete description

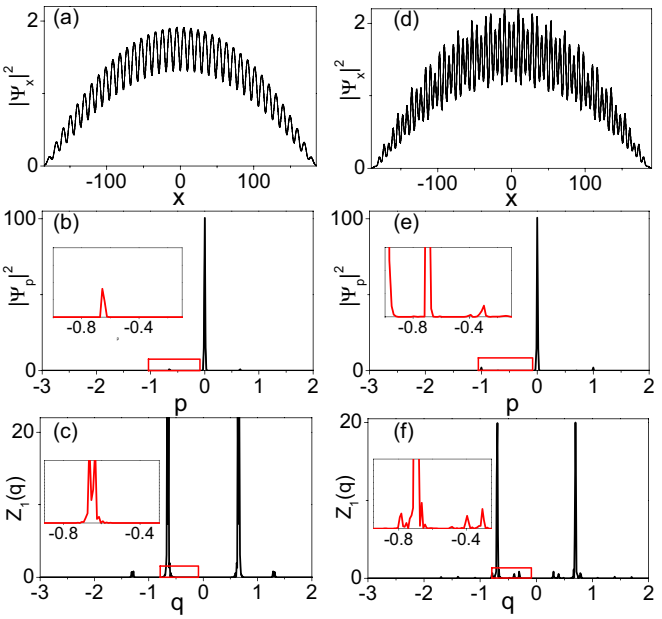

FIG. 4. Space density along x direction [(a) and (d)], momentum density of $\psi_p = 1/\sqrt{L_x}\int dx\, e^{-ipx}|\psi_x|^2$ [(b) and (e)], and the corresponding static structure factor Z_1 [(c) and (f)] of an optically trapped SOC BEC in the mixed phase. The x and p (or q) are in units of $1/(2k_L)$ and $2k_L$, respectively. The dimensionless parameters γ, Ω, c, and c_{12} read $\gamma = 2k_R/k_L$, $\Omega \to \Omega/8E_L$ $c = N\hbar\omega_\perp k_L a_{11}/(4\pi N_d E_L)$, and $c_{12} = N\hbar\omega_\perp k_L a_{12}/(4\pi N_d E_L)e^{-d^2/a_\perp^2}$. We take $\gamma = 0.35$, $c = 0.1$, $c_{12} = 0.08$, $\Omega = 0.1$, and $v = 0$ [(a)–(c)]; $\Omega = 0.04$, $v = 0.1$ [(d)–(f)]. A weak harmonic trap with the trap frequency $\hbar\omega_x/8E_L = 0.003$ is included in the numerical calculations.

of how to probe the ground-state phase diagram of an optically trapped SOC BEC in the superfluid regime by Bragg spectroscopy.

We now detail our discussions on the Bragg spectroscopy of a SOC BEC in an OL. Let us first describe as a reference the Bragg spectroscopy of a lattice-free SOC BEC in the stripe phase. Both our results for the density profile along the x direction [see Fig. 4(a)] and the static structure factor Z_1 as a function of q [see Fig. 4(c)] are consistent with Ref. [20]: the density profile exhibits periodic modulation, and the structure factor is divergent around $\pm 2k_1 \sim 0.7$ [see Fig. 4(c)], both being the characteristic features of the stripe phase with spontaneously broken continuous symmetries. By contrast, the inclusion of an OL ($v \neq 0$) results in complicated density distribution [see Fig. 4(d)], where an obvious periodicity is absent [48]. Unlike the uniform counterpart, in particular, the structure factors Z_1 for the lowest level [see Fig. 4(f)] exhibit multiple peaks at momenta $\sim\pm 0.7, \pm 0.3, \pm 0.4$, which can be seen as a signature for the mixed phase which lacks the periodicity. This phenomena can be understood in a similar spirit as Ref. [20]: there exists inequalities of $m_0(F)m_0(G) \geqslant |\langle [F,G]\rangle|^2$ with $m_0(F) = \sum_l(|\langle 0|F|l\rangle|^2 + |\langle 0|F^\dagger|l\rangle|^2)$. Here we choose the operators $F = \sum_j e^{iqx_j}$ and $G = \sum_j (p_x e^{-i(q-q_B)x_j} + \text{H.c.})/2$ with q_B being the arbitrary momentum to be determined. Then, the commutator $\langle [F,G]\rangle = q_x N\langle e^{iq_B x}\rangle$ is proportional to the density modulations of the mixed phase, which are plotted in Fig. 4(b) for $v = 0$ and Fig. 4(e) for $v \neq 0$, respectively.

Without the OL ($v = 0$), $\langle e^{iq_B x}\rangle$ is nonzero at $q_B = 2k_1$. In this case, the $m_0(F)$ and $m_0(G)$ can be shown to be proportional to $Z_1(q)$ and $|q - q_B|$ in the first Brillioun zone, respectively, resulting in a divergence of Z_1 around $2k_1$. In contrast, adding an OL ($v \neq 0$) can give rise to a mixed state which is nonperiodic [48]. In addition, due to the appearance of multiple peaks in $\langle e^{iq_B x}\rangle$ at $\pm 0.3, \pm 0.4$ [see Fig. 4(e)], the structure factor at these momenta becomes divergent [see Fig. 4(f)]. We conclude that the appearance of multiple peaks beyond $2k_1$ in the structure factor can serve as a criterion for the identification of the mixed phase studied in this work.

V. EXPERIMENTAL ASPECTS

The experimental realization of the phase diagram studied in this work requires control of five parameters: the SOC parameters γ and Ω, the lattice strength v, and the interatomic interactions c and c_{12}. In current experiments [5], the relevant experimental parameters are given as follows. The wave vectors of generating the OL and SOC reads $k_L = 2\pi/\sqrt{2}\lambda_L$ with $\lambda_L = 1540$ nm and $k_R = 2\pi/\sqrt{2}\lambda_R$ with $\lambda_R = 784$ nm, respectively, leading to a dimensionless SOC parameter $\gamma = k_R/2k_L = 0.98$. The γ can be further tuned by the method of shaking [49,50]: a *fast* coherent modulation of the Raman coupling $\Omega = \Omega_0 + \Delta\Omega\cos(\omega_0 t)$ gives rise to a modified SOC parameter such that $\gamma \to \gamma J_0(\Delta\Omega/\omega_0)$, thus allowing a control of γ via varying the laser parameters. The detuning δ and the Rabi frequency Ω are free parameters and in the experiment they can be tuned by changing of frequency difference and the intensity of Raman beams, respectively. The lattice strength in Ref. [5] is set by $V_0 = -1.4E_L$, corresponding to the dimensionless parameter $v = 0.09$. Moreover, v can be easily varied from 0 to 0.5 provided the BEC is in the superfluid regime [5] (corresponding to a lattice strength of V_0 from $0E_L$ to $8E_L$). In addition, the typical values of ratio $c_{ij} = \frac{N\hbar\omega_\perp k_L a_{ij}}{4\pi N_d E_L}(i = j)$ range from 0 to 0.2 and the variation of g_{ij} can be achieved in a very versatile manner by optical Feshbach resonance [51] or confined induced resonance. The ratio of c/c_{12} can be adjusted as $c/c_{12} = \exp(-d^2/a_\perp^2)$ by changing the relative displacement d of the two-component densities located in the harmonic trap.

Upon reaching the aforementioned parameter regimes, central to testing the validity of the physics in this article concerns the experimental realization of an optically trapped SOC BEC in superfluid phase in the crossover from 3D to quasi-1D. The present facilities have allowed that a quasi-1D BEC without SOC and superfluidity can be both achieved below a critical temperature at the nodes of 2D optical lattice potentials. Furthermore, adding SOC to a quasi-1D BEC allows one to combine the benefit of the reduced dimensionality with the advantage of working with large, yet coherent samples. Therefore, the predicted phase diagram of an optically trapped Bose gas here is expected to be observable within the current experimental capabilities.

Finally, we should bear in mind the assumptions that underly our results. First, our study is based on the Gross-Pitaevskii mean-field theory. Theoretically, it has been established that, at the mean-field level, the Gross-Pitaevskii theory can well describe both the static and dynamic properties of a BEC with SOC. The validity of the Gross-Pitaevskii equation can be tested a *posteriori* by evaluating the quantum depletion of the condensate as shown in Appendix A. For a more rigorous proof of the validity of Gross-Pitaevskii equation in uniform case, we refer to the Supplemental Material in Ref. [52]. Second, our treatment is limited to the superfluid regime [53], where the lattice strength v is tuned below the critical value above which the system is supposed to be in the Mott phase.

VI. CONCLUSION AND OUTLOOK

In summary, we have obtained the ground-state phase diagram of a SOC BEC trapped in a 1D OL, where three normal phases and one mixed phase are identified. We find that while for a weak OL the phase diagram resembles its uniform counterpart, a strong OL will lead to significant modifications. In particular, the ground state of the mixed phase is represented by a superposition of two Bloch waves with the opposite Bloch vector k_1, which involves an interplay between the periodicity of the OL and the periodicity due to the SOC. Remarkably, when these two periods are incommensurate, the ground state exhibits no periodicity even though the system's Hamiltonian is periodic. We hope this work can contribute to the ongoing experiments of loading a SOC BEC into an OL.

ACKNOWLEDGMENTS

We thank Libin Fu, Biao Wu, Liming Guan, Ying Hu, Qizhong Zhu, Xiongjun Liu, and W. Vincent Liu for stimulating discussions. Z.C. is supported by the NSFC of China (Grant No. 11404026). Z.X.L. is supported by the NSFC of China (Grant No. 11274315) and Youth Innovation Promotion Association CAS (Grant No. 2013125).

APPENDIX A: VALIDITY OF GROSS-PITAEVSKII MEAN-FIELD THEORY

Here, we justify the Gross-Pitaevskii mean-field approximation used in this work *a posteriori* by evaluating the quantum depletion. For a uniform BEC, the quantum depletion is $\sim\sqrt{na^3}$ and the mean-field approximation is valid provided $na^3 \ll 1$. While this result is modified by a prefactor $(k_R^2/gn)^{1/4}$ [18] in a SOC BEC, the quantum depletion remains small for the relevant experimental parameters and can be safely ignored. On the other hand, for an optically trapped quasi-1D SOC BEC studied in this work, in addition to the phase fluctuations due to the tight confinement along y and z directions, the effect of a strong lattice potential can also increase quantum fluctuations and thus affect the mean-field approximation. Nevertheless, as we will show below, for the considered parameter regimes, the quantum depletion of the model system remains sufficiently small, which justifies the mean-field description.

Our starting point is the 3D Gross-Piteavskii equation derived by variation of the energy functional (1) with respect to $\Psi^\dagger$

$$i\hbar\frac{\partial\Psi}{\partial t} = \Big[H_0 + V_{ext}(\mathbf{r}) + \frac{1}{2}(g + g_{12})\Psi^\dagger\Psi + \frac{1}{2}(g - g_{12})(\Psi^\dagger\sigma_z\Psi)\sigma_z\Big]\Psi. \quad \text{(A1)}$$

We first apply the Bogoliubov theory to Eq. (A1) and decompose the 3D condensate wave function $\Psi(\mathbf{r})$ into the ground-state wave function $\Psi_0(\mathbf{r})$ and a small fluctuating term $\delta\Psi(\mathbf{r})$ reading

$$\delta\Psi(\mathbf{r}) = e^{-i\mu t/\hbar}\left[\begin{pmatrix}U_1(\mathbf{r})\\U_2(\mathbf{r})\end{pmatrix}e^{-i\omega t} + \begin{pmatrix}V_1(\mathbf{r})\\V_2(\mathbf{r})\end{pmatrix}e^{i\omega t}\right]. \quad \text{(A2)}$$

Due to the strong transverse confinement which freezes the atomic motion along these directions, the fluctuating amplitudes of $U_i(\mathbf{r})$ and $V_i(\mathbf{r})$ $(i = 1,2)$ can be simplified into $U_i(\mathbf{r}) = u_i(x)\phi(y,z)$ and $V_i(\mathbf{r}) = v_i(x)\phi(y,z)$ with $\phi = (\phi_-,\phi_+)^T$ and $\phi_\pm = 1/(\sqrt{\pi}a_\perp)e^{-[(y\pm d/2)^2+(z\pm d/2)^2]/2a_\perp^2}$. Substituting Eq. (A2) into Eq. (A1) and expanding $u_i(x)$ and $v_i(x)$ in the Bloch form, we obtain the dimensionless Bogoliubov–de Gennes equations (9) in the main text. By solving Eqs. (9) numerically, both the Bogoliubov excitation spectrum and the amplitudes in Eq. (A2) can be extracted. Then the quantum depletion of SOC BEC is given by

$$\frac{\Delta N}{N} = \frac{1}{N}\sum_j \sum_{i=1,2} \sum_{\mathbf{q}} \int d^3r \left|V^j_{\mathbf{q},i}(\mathbf{r})\right|^2, \quad \text{(A3)}$$

where N denotes the total number of atoms, ΔN is the number of noncondensed particles, and $V^j_{\mathbf{q},i}(\mathbf{r})$ are the 3D Bogoliubov amplitudes of the elementary excitations. The summation involves all Bogoliubov bands j with $i = 1,2$ labeling the two-component amplitude, and the quasimomenta $\mathbf{q}$ in the first Brillouin zone. Note that we set $q_y = q_z = 0$ in our detailed calculations, because the strong transverse confinement freezes the fluctuations in these directions.

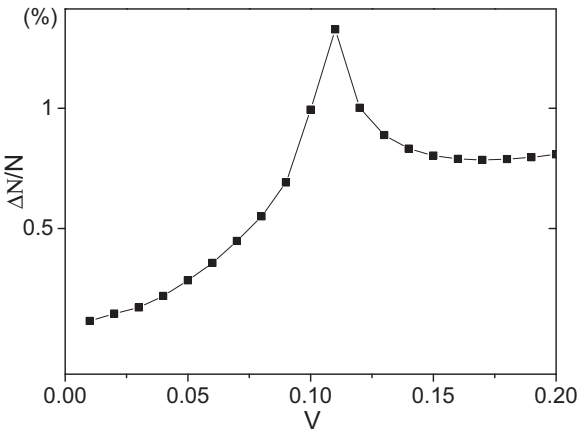

FIG. 5. Quantum depletion as a function of the lattice strength v. Here, the lattice strength v is in units of $-16E_L$. The quantum depletion is always less than 2%, thereby confirming the validity of the Gross-Piteavskii mean-field theory. In our numerical simulations, we have chosen a quasi-1D SOC BEC with the s-wave scattering length of $k_L a_{11} = k_L a_{12} = 3.1 \times 10^{-4}$, which consists of $\sim 2\pi \times 10^4$ atoms that are confined in a trap with frequency $\omega_\perp = 10 \times E_L/h$ in transverse directions. Here, we choose the experimental parameters: $k_L = 2\pi/\sqrt{2}\lambda_L$ with $\lambda_L = 1540$ nm and $E_L = h \times 483$ Hz in Ref. [5]. Along x direction, the SOC is subjected to an OL consisting of ~ 100 lattice well, i.e., $\sim 2\pi \times 10^2$ atoms per well. Other parameters are $\gamma = k_R/(2k_L) = 0.4$, $\Omega \to \Omega/8E_L = 0.25$, and $c = c_{12} = N\hbar\omega_\perp k_L a_{11}/(4\pi N_d E_L) = 0.05$.

In Fig. 5, we present the quantum depletion $\delta N/N$ as a function of the periodic potential depth v, taking typical experimental parameters. For the parameters relevant in our work, we have verified that the quantum depletion is always less than 2%, thereby confirming the validity of the Gross-Pitaevskii approach.

APPENDIX B: VALIDITY OF ANSATZ (4)

In this section, we discuss the validity of the ansatz (4), based on which we have derived the ground-state phase diagram of an optically trapped BEC. To put our discussion into perspective, we note that for a SOC BEC without lattice, the ansatz (4) is not the stationary solution of the Gross-Pitaevskii equation in the stripe phase. As pointed out by Ref. [20], this ansatz has neglected the high-order harmonics of the condensate wave function generated by the interatomic interactions, which is analogous to the frequency doubling in nonlinear optics [54,55]. Specifically, the condensate will not only occupy the $\pm k_1$ states, but also the states with momenta $\pm 3k_1$, $\pm 5k_1$, etc., which result in corrections to the

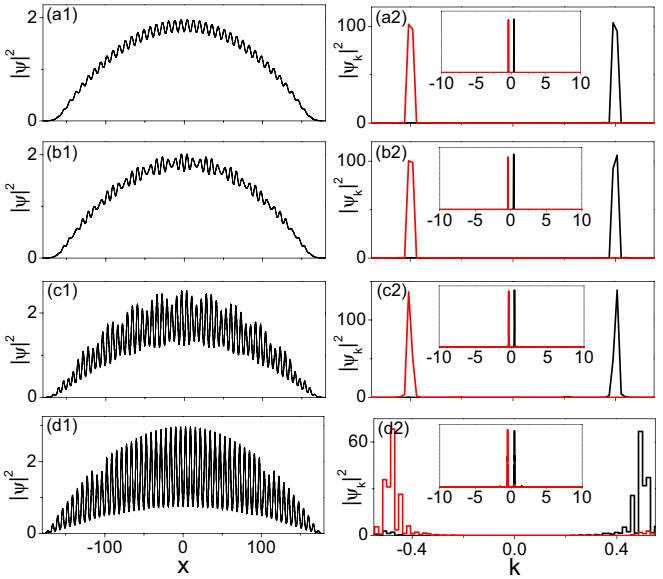

FIG. 6. Left panel: density profile along the x direction for lattice strength $v = 0$ (a1), $v = 0.01$ (b1), $v = 0.1$ (c1), and $v = 0.2$ (d1). Right panel: momentum density profile along the momentum k with the different lattice strength of $v = 0$ (a2), $v = 0.01$ (b2), $v = 0.1$ (c2), and $v = 0.2$ (d2). The x, p, and v are in units of $1/(2k_L)$, $2k_L$, and $-16E_L$, respectively. In our numerical simulations, we have chosen a quasi-1D SOC BEC with the s-wave scattering length of $k_L a_{11} = 3.1 \times 10^{-4}$ and $k_L a_{12} = 2.5 \times 10^{-4}$, consisting of $\sim 2\pi \times 10^4$ atoms confined in a trap with a transverse trapping frequency $\omega_\perp = 10 \times E_L/h$. We take typical experimental parameters $k_L = 2\pi/\sqrt{2}\lambda_L$, with $\lambda_L = 1540$ nm and $E_L = h \times 483$ Hz in Ref. [5]. In the x direction, the SOC is subjected to an OL with ~ 100 lattice well, and therefore, there are $\sim 2\pi \times 10^2$ atoms on the average in each well. For other parameters, we take $\gamma = k_R/(2k_L) = 0.4$, $\Omega \to \Omega/8E_L = 0.03$, $c = N\hbar\omega_\perp k_L a_{11}/(4\pi N_d E_L) = 0.05$, and $c_{12} = N\hbar\omega_\perp k_L a_{12}/(4\pi N_d E_L)e^{-d^2/a_\perp^2} = 0.04$. For the weak harmonic trap along the x direction, we choose the trapping frequency $\omega_x/8E_L = 0.0025$.

energy density obtained from the ansatz (4). These corrections are usually small, in particular when the density is not very high and interaction strength is small, and will only become pronounced in the stripe phase where they need to be properly taken into account. However, when an OL is present (particularly for strong OL), where the plane-wave functions are Bragg refracted to form Bloch waves, it is expected these correction can influence the entire phase diagram. The improved ansatz for the energy functional (3) including all these effects can be assumed as

$$\begin{aligned}\psi_t &= \sum_{l=0,1,\ldots} \{\psi_{(2l+1)k_1} + \psi_{-(2l+1)k_1}\} \\ &= \sum_m \left\{ \begin{pmatrix} a_{1m} \\ b_{1m} \end{pmatrix} e^{i(k_1+m)x} + \begin{pmatrix} a_{2m} \\ b_{2m} \end{pmatrix} e^{i(-k_1+m)x} \right. \\ &\quad \left. + \begin{pmatrix} a_{3m} \\ b_{3m} \end{pmatrix} e^{i(3k_1+m)x} + \begin{pmatrix} a_{4m} \\ b_{4m} \end{pmatrix} e^{i(-3k_1+m)x} + \cdots \right\}. \quad \text{(B1)}\end{aligned}$$

Thus ansatz (4) in the main text corresponds to a truncation of Eq. (B1) to the first term with $l = 0$, with higher-order terms ignored. Below we verify the validity of such truncation, by numerically solve Gross-Pitaevskii equation with imaginary time algorithm.

Figure 6 presents the numerical results of space and momentum density profiles for $\gamma = 0.4$ (corresponding to $\cos\theta = 0.93$ and $k_1 = 0.4$). Note that for $v = 0$, the ansatz (4) is expected to reduce to Eq. (5) describing the stripe phase of a uniform SOC BEC. This is also confirmed by our direct numerical calculation for the momentum density [Fig. 6(a2)], which clearly display two peaks around $\pm k_1$. The cases with OLs are shown in Figs. 6(b2)–6(d2), where we have considered the lattice strength $v = 0.01$, 0.1, and 0.2. We see that when the lattice is weak, there are two sharp peaks at around $\pm k_1$. When lattice strength increases, the two peaks at $\pm k_1$ remain dominant compared to other emerging peaks (note that for $v = 0.2$, k_1 is shifted to 0.49 due to strong periodic modulation). This suggests that we can neglect the contributions of the high-order harmonics of the condensate wave function generated by the nonlinear interactions. We thus conclude within our calculation that the ansatz (4) provides a satisfactory description of our model system for v up to 0.2.

[1] J. Dalibard, F. Gerbier, G. Juzeliūnas, and P. Öhberg, Rev. Mod. Phys. **83**, 1523 (2011).
[2] H. Zhai, Int. J. Mod. Phys. B **26**, 1230001 (2012).
[3] H. Zhai, Rep. Prog. Phys. **78**, 026001 (2015).
[4] V. Galitski and I. B. Spielman, Nature (London) **494**, 49 (2013).
[5] C. Hamner, Y. Zhang, M. A. Khamehchi, M. J. Davis, and P. Engels, Phys. Rev. Lett. **114**, 070401 (2015).
[6] C. Nayak, S. H. Simon, A. Stern, M. Freedman, and S. Das Sarma, Rev. Mod. Phys. **80**, 1083 (2008).
[7] M. Z. Hasan and C. L. Kane, Rev. Mod. Phys. **82**, 3045 (2010).
[8] X.-L. Qi and S.-C. Zhang, Rev. Mod. Phys. **83**, 1057 (2011).
[9] W. S. Cole, S. Zhang, A. Paramekanti, and N. Trivedi, Phys. Rev. Lett. **109**, 085302 (2012).
[10] S. Mandal, K. Saha, and K. Sengupta, Phys. Rev. B **86**, 155101 (2012).
[11] J. Radić, A. Di Ciolo, K. Sun, and V. Galitski, Phys. Rev. Lett. **109**, 085303 (2012).
[12] C. H. Wong and R. A. Duine, Phys. Rev. Lett. **110**, 115301 (2013).
[13] D.-W. Zhang, J.-P. Chen, C.-J. Shan, Z. D. Wang, and S.-L. Zhu, Phys. Rev. A **88**, 013612 (2013).
[14] W. Han, G. Juzeliunas, W. Zhang, and W.-M. Liu, Phys. Rev. A **91**, 013607 (2015).
[15] J. Larson, J.-P. Martikainen, A. Collin, and E. Sjöqvist, Phys. Rev. A **82**, 043620 (2010).
[16] Z. Cai, X. Zhou, and C. Wu, Phys. Rev. A **85**, 061605 (2012).
[17] T.-L. Ho and S. Zhang, Phys. Rev. Lett. **107**, 150403 (2011).
[18] Y. Li, L. P. Pitaevskii, and S. Stringari, Phys. Rev. Lett. **108**, 225301 (2012).
[19] G. I. Martone, Y. Li, L. P. Pitaevskii, and S. Stringari, Phys. Rev. A **86**, 063621 (2012).
[20] Y. Li, G. I. Martone, L. P. Pitaevskii, and S. Stringari, Phys. Rev. Lett. **110**, 235302 (2013).
[21] G. I. Martone, Y. Li, and S. Stringari, Phys. Rev. A **90**, 041604 (2014).
[22] W. Li, L. Chen, Z. Chen, Y. Hu, Z. Zhang, and Z. Liang, Phys. Rev. A **91**, 023629 (2015).
[23] Y. Zhang and C. Zhang, Phys. Rev. A **87**, 023611 (2013).
[24] Y. J. Lin, R. L. Compton, K. Jimenez-Garcia, J. V. Porto, and I. B. Spielman, Nature (London) **462**, 628 (2009).
[25] Y. J. Lin, K. Jimenez-Garcia, and I. B. Spielman, Nature (London) **471**, 83 (2011).
[26] P. Wang, Z.-Q. Yu, Z. Fu, J. Miao, L. Huang, S. Chai, H. Zhai, and J. Zhang, Phys. Rev. Lett. **109**, 095301 (2012).
[27] L. W. Cheuk, A. T. Sommer, Z. Hadzibabic, T. Yefsah, W. S. Bakr, and M. W. Zwierlein, Phys. Rev. Lett. **109**, 095302 (2012).
[28] We would like to point out that the Raman coupling in the case of the large value of Ω will modify the condensate wave function by increasing the overlap of the two spin states. In such, the expression for $\phi_\pm$ may be no longer valid. But this will not change the main result, e.g., phase diagram of the current paper, as these results are not directly related to the form of $\phi_\pm$.
[29] B. Wu and Q. Niu, Phys. Rev. A **64**, 061603 (2001).
[30] A. Smerzi, A. Trombettoni, P. G. Kevrekidis, and A. R. Bishop, Phys. Rev. Lett. **89**, 170402 (2002).
[31] M. Machholm, C. J. Pethick, and H. Smith, Phys. Rev. A **67**, 053613 (2003).
[32] S. Burger, F. S. Cataliotti, C. Fort, F. Minardi, M. Inguscio, M. L. Chiofalo, and M. P. Tosi, Phys. Rev. Lett. **86**, 4447 (2001).
[33] L. Fallani, L. De Sarlo, J. E. Lye, M. Modugno, R. Saers, C. Fort, and M. Inguscio, Phys. Rev. Lett. **93**, 140406 (2004).
[34] D. M. Stamper-Kurn, A. P. Chikkatur, A. Görlitz, S. Inouye, S. Gupta, D. E. Pritchard, and W. Ketterle, Phys. Rev. Lett. **83**, 2876 (1999).
[35] R. Ozeri, N. Katz, J. Steinhauer, and N. Davidson, Rev. Mod. Phys. **77**, 187 (2005).
[36] P. T. Ernst, S. Gotze, J. S. Krauser, K. Pyka, D.-S. Luhmann, D. Pfannkuche, and K. Sengstock, Nat. Phys. **6**, 56 (2010).

[37] X. Du, S. Wan, E. Yesilada, C. Ryu, D. J. Heinzen, Z. Liang, and B. Wu, New J. Phys. **12**, 083025 (2010).
[38] D. Clément, N. Fabbri, L. Fallani, C. Fort, and M. Inguscio, Phys. Rev. Lett. **102**, 155301 (2009).
[39] L. Chen, W. Li, Z. Chen, Z. Zhang, and Z. Liang, J. Low Temp. Phys. **177**, 291 (2014).
[40] L. Chen, Z. Chen, W. Li, Z. Zhang, and Z. Liang, Eur. Phys. J. D **68**, 375 (2014).
[41] Z. X. Liang, X. Dong, Z. D. Zhang, and B. Wu, Phys. Rev. A **78**, 023622 (2008).
[42] P. A. Ruprecht, M. Edwards, K. Burnett, and C. W. Clark, Phys. Rev. A **54**, 4178 (1996).
[43] P. B. Blakie, R. J. Ballagh, and C. W. Gardiner, Phys. Rev. A **65**, 033602 (2002).
[44] F. Zambelli, L. Pitaevskii, D. M. Stamper-Kurn, and S. Stringari, Phys. Rev. A **61**, 063608 (2000).
[45] M. A. Khamehchi, Y. Zhang, C. Hamner, T. Busch, and P. Engels, Phys. Rev. A **90**, 063624 (2014).
[46] L.-C. Ha, L. W. Clark, C. V. Parker, B. M. Anderson, and C. Chin, Phys. Rev. Lett. **114**, 055301 (2015).
[47] S.-C. Ji, L. Zhang, X.-T. Xu, Z. Wu, Y. Deng, S. Chen, and J.-W. Pan, Phys. Rev. Lett. **114**, 105301 (2015).
[48] Note that there exist two kinds of possibilities regarding periodicity of the wave function being lacking in Fig. 4(d). On the one hand, in the case of two periods being incommensurate, the ground state is not a Bloch wave. On the other hand, it's also expected that with two different periods superimposed, the system is still periodic, just with larger period. In particular, when such a period is larger than the system's size, the system becomes nonperiodic within the system's size.
[49] Y. Zhang, G. Chen, and C. Zhang, Sci. Rep. **3**, 1937 (2013).
[50] K. Jiménez-García, L. J. LeBlanc, R. A. Williams, M. C. Beeler, C. Qu, M. Gong, C. Zhang, and I. B. Spielman, Phys. Rev. Lett. **114**, 125301 (2015).
[51] C. Chin, R. Grimm, P. Julienne, and E. Tiesinga, Rev. Mod. Phys. **82**, 1225 (2010).
[52] T. Ramos, H. Pichler, A. J. Daley, and P. Zoller, Phys. Rev. Lett. **113**, 237203 (2014).
[53] C. Menotti, M. Krämer, L. Pitaevskii, and S. Stringari, Phys. Rev. A **67**, 053609 (2003).
[54] M. Machholm, A. Nicolin, C. J. Pethick, and H. Smith, Phys. Rev. A **69**, 043604 (2004).
[55] A. Maluckov, G. Gligorić, L. Hadzievski, B. A. Malomed, and T. Pfau, Phys. Rev. Lett. **108**, 140402 (2012).